

Check for updates



Perturbation of Anion/Cation Transport Leads to Apical Panicle Abortion in Rice by Disrupting Ca²⁺ Homeostasis

Bojuan Liu¹ | Sheng Luo¹ | Wang Tian² | Xin Liu^{1,3} | Jinhui Zhang¹ | Yulong Ren¹ | Zebin Liu⁴ | Jiale Shao¹ | Yangi Chang¹ | Zhijun Cheng^{1,3} | Jianmin Wan^{1,5,6} [D

¹State Key Laboratory of Crop Gene Resources and Breeding, Institute of Crop Sciences, Chinese Academy of Agricultural Sciences, Beijing, China | ²State Key Laboratory of Protein and Plant Gene Research, School of Advanced Agricultural Sciences, Peking University, Beijing, China | 3Nanfan Research Institute, Chinese Academy of Agricultural Sciences, Sanya, Hainan, China | 4College of Life Science, Capital Normal University, Beijing, China | 5State Key Laboratory for Crop Genetics and Germplasm Enhancement, Nanjing Agricultural University, Nanjing, China | 6Zhongshan Biological Breeding Laboratory, Nanjing, China

Correspondence: Zhijun Cheng (chengzhijun@caas.cn) | Jianmin Wan (wanjianmin@caas.cn)

Received: 2 July 2025 | Revised: 18 September 2025 | Accepted: 22 September 2025

Funding: This research was supported by grants from the Biological Breeding National Science and Technology Major Project (2023ZD0406802), the National Nanfan Research Institute project of CAAS (YBXM2563), the National Key Research and Development Program of China (2022YFF1002903) and the Agricultural Science and Technology Innovation Program (CAAS ZDRW202401).

Keywords: rice | panicle apical abortion | calcium ion homeostasis | PAA2 | OsUBC45

ABSTRACT

Calcium ion (Ca²⁺) is an essential plant nutrient required for cell structure establishment, as well as a counter-cation of an anion and an intracellular messenger. Calcium is absorbed from soil by roots and delivered to shoots through the xylem. The process must be finely balanced to avoid excessive accumulation. However, the regulatory mechanisms involved in calcium homeostasis remain unclear. In this study, we identified a gain-of-function mutant of paa2, a member of the NITRATE TRANSPORTER1/ PEPTIDE TRANSPORTER family (NPF), that acts as a symporter of NO₃⁻ and other cations. Ca²⁺ and some other cations were over-accumulated in the apex of developing panicles in both the gain-of-function mutant paa2 and PAA2 overexpressing plants. Apical panicle abortion in the paa2 mutant was mainly caused by excessive calcium accumulation. PAA2 was preferentially expressed in various meristic tissues during panicle development. PAA2 was found in the plasma membrane, endoplasmic reticulum (ER) and prevacuolar compartment, and co-localised with the vesicle-associated membrane protein 727 (VAMP727), implying that it transported calcium ions into and out of cells. Our study revealed that the tip-orientated calcium gradient in the panicle is controlled coordinately by the PAA2-UBC45 module. These findings suggest that PAA2 is a key player in maintaining Ca²⁺ homeostasis during panicle development in rice.

1 | Introduction

The calcium ion (Ca²⁺) is an essential macronutrient, as well as a universal second messenger in regulating plant growth and in responding to extracellular stimuli (Dong et al. 2022; Wang, Chen, et al. 2023). The concentration of cytoplasm-free Ca²⁺ in plant cells is usually maintained at about 100-200 nM (Helper 2005; Jezek and Blatt 2017). To maintain cellular homeostasis of Ca²⁺, plant cells have evolved an intricate mechanism that utilises the intracellular organelles such as the endoplasmic reticulum (ER) and vacuole lumen as a regulatory pool to cope with changes in Ca²⁺ concentration in the external environment (Gilliham et al. 2011; Wang and Luan 2024). Ca²⁺ deficiency can hinder the formation of cell walls, cause instability of cell membranes and

Bojuan Liu, Sheng Luo, Wang Tian, Xin Liu and Jinhui Zhang contributed equally to this study.

This is an open access article under the terms of the Creative Commons Attribution-NonCommercial-NoDerivs License, which permits use and distribution in any medium, provided the original work is properly cited, the use is non-commercial and no modifications or adaptations are made.

© 2025 The Author(s). Plant Biotechnology Journal published by Society for Experimental Biology and The Association of Applied Biologists and John Wiley & Sons

increase the permeability of cell membranes, seriously affecting plant growth (Thor 2019; White and Broadley 2003). Conversely, excessive intracellular Ca^{2+} concentration has cytotoxicity, typically leading to cell death and inhibited growth (Hepler and Wayne 1985; Orrenius et al. 2003; Kamiya et al. 2006; Huang et al. 2016; Wang et al. 2024; Zhou et al. 2024).

The rice panicle is a limited growth inflorescence that differentiates from the stem apex during the transition from vegetative to reproductive growth. Panicle development initiates with cell division and expansion in the apical inflorescence meristem, followed by the formation of primary rachis branches, secondary rachis branches and finally lateral spikelet meristems. After the completion of panicle differentiation (at less than 4cm in length), subsequent developmental stages mainly involve rapid rachis elongation and maturation of reproductive organs (Ikeda et al. 2004). The role of calcium in rice panicle development is well documented. Peng et al. (2018) observed that a mutation in the calcineurin Blike protein-interacting protein kinase 31 gene (OsCIPK31) caused excessive ROS accumulation, eventually leading to the abortion of florets in the distal part of the inflorescence, the panicle apical abortion (PAA) phenotype. A mutation in the OsCAX1a gene that encodes a Ca2+/H+ exchanger caused apex Ca2+ deficiency and spikelet degeneration, indicating a crucial role of Ca2+ in maintaining optimal calcium concentration in panicle development (Gan et al. 2023). The acropetal (proximal-distal) extension pattern of a developing panicle mimics the polarised growth in single cells such as root hairs and pollen tubes, where the more active distal portion in the cell accumulates calcium and results in a tipfocused gradient of cytosolic Ca2+ (Palanivelu and Preuss 2000; Hepler et al. 2001; Tian et al. 2020). However, it is currently unclear whether there is a similar calcium gradient in multicellular tissues such as rapidly developing young panicles.

The exact mechanism of long-distance acropetal transportation of Ca²⁺ is unknown; a common viewpoint is that the long-distance movement of Ca2+ in land plants is a process of passive uptake pulled through the xylem by transpiration (Wang and Luan 2024). To maintain electroneutrality, land plants adopt a so-called cation-anion balance mechanism, by which accumulation of cations, that is, K⁺, Ca²⁺, Mg²⁺, parallels an increase in anion levels (NO₂⁻, SO₄²⁻, H₂PO₄⁻, Cl⁻), with NO₃⁻ (nitrate) considered the main factor stimulating cation uptake (Kirkby and Knight 1977). Nitrate is the major nitrogen source for most land plants. Several plasma membrane-localised NPF proteins in Arabidopsis, including AtNPF7.3/NRT1.5, AtNPF7.2/NRT1.8, AtNPF2.3 and AtNPF2.9/ NRT1.9 (Lin et al. 2008; Li et al. 2010; Taochy et al. 2015; Wang and Tsay 2011) are considered to be nitrate root-to-shoot transporters and shoot homeostasis of potassium (K). NRT1.5 was characterised as a proton-coupled H+/K+ antiporter responsible for NO₃⁻-dependent K⁺ transportation and K⁺ loading into the xylem (Drechsler et al. 2015; Li et al. 2017). Its homologue NRT1.8 functioned in mediating low-affinity nitrate uptake, and the mutant nrt1.8-1 showed a nitrate-dependent Cd²⁺-sensitive phenotype (Li et al. 2010). These reports highlight the role of NRT1.5 and NRT1.8 in maintaining cation-anion balance, but whether they are involved in calcium ion homeostasis or long-distance transport remains to be determined.

In a study on the mechanism underlying PAA in a gain-function mutant *paa2*, we found that overexpression of *PAA2*, a rice gene

homologue of both *NRT1.5* and *NRT1.8*, caused tip-focused accumulation of cations, and that excessive Ca^{2+} was the main factor responsible for the PAA phenotype. Our results indicated that PAA2 can transport Ca^{2+} and other cations, but its role is constrained by E2 ubiquitin conjugating enzyme OsUBC45 interaction with PAA2 to maintain Ca^{2+} homeostasis in panicles. Moreover, we demonstrated the presence of a Ca^{2+} gradient at the time of young panicle elongation, suggesting a crucial role of Ca^{2+} in panicle development.

2 | Results

2.1 | Map-Based Cloning of Gene PAA2

The paa2 mutant, a T-DNA insertion mutant, was identified from a HTF (hybrid transcription factor) library (Zhao et al. 2015). Compared with its wild-type cv. Kitaake (WT), the paa2 mutant has 58% aborted spikelets, mostly located at the distal end of the panicle (Figure 1A-D), as well as other changes, including delayed heading, reduced plant height and tiller number, fewer grains per panicle, smaller grain size and lower grain weight (Figure S1). To clone the causative gene, we constructed a mapping population by hybridising the paa2 mutant with japonica cultivar IRAT129. The PAA2 locus was finally narrowed down to a 49.7 kb interval containing four open reading frames (ORFs), viz., LOC_Os02g46420 (ORF1), LOC_Os02g46440 (ORF2), LOC_ Os02g46450 (ORF3) and LOC_Os02g46460 (ORF4). Genomic sequence comparisons revealed no variation except a T-DNA insertion 1kb upstream of LOC_Os02g46460 (Figure 1E). The insertion caused increased expression of the genes in this interval relative to WT, with the highest increment (23-fold in leaves and 128-fold in panicles) for LOC_Os02g46460 (Figures 1F and S2). The candidate gene was confirmed by introducing a LOC Os02g46460-RNA interference (RNAi) vector into the paa2 mutant and overexpressing LOC_Os02g46460 driven by the rice ubiquitin promoter in Japonica cv. Zhonghua11 (ZH11) and Nipponbare (NIP), respectively. RNAi transgenic lines of the paa2 mutant recovered a normal phenotype (Figure 1G,J), and the LOC_Os02g46460 overexpression lines had a phenotype similar to the paa2 mutant (Figures 1H,I,K,L and S3). Hereafter we designated LOC_Os02g46460 as PAA2 (Panicle Apical Abortion on Chromosome 2).

2.2 | Overexpression of *PAA2* Causes Increased Nitrogen Concentration and Excessive Accumulation of Calcium and Other Cations

PAA2 belongs to the rice NPF protein family OsNPF7.9, with high identity to the Arabidopsis AtNRT1.5/AtNPF7.3 and AtNRT1.8/AtNPF7.2. Previous research revealed that PAA2 is a low-affinity nitrate transporter, participating in nitrogen relocation from roots to shoots (Guan et al. 2022). Given the possibility of PAA2 transporting N and other cations acropetally, and to identify substances associated with PAA, we measured the concentrations of nutrients in transgenic ZH11 plants overexpressing *PAA2* (*PAA2*-OE^{ZH11}). Compared with the wild type, nitrogen accumulated in whole *PAA2*-OE^{ZH11} plants (Figure 2A) and there were excessive accumulations of several cations (Ca²⁺, Mg²⁺, Mn²⁺, K⁺, Na⁺, Zn²⁺, Fe²⁺ etc.) in panicles (Figure 2B).

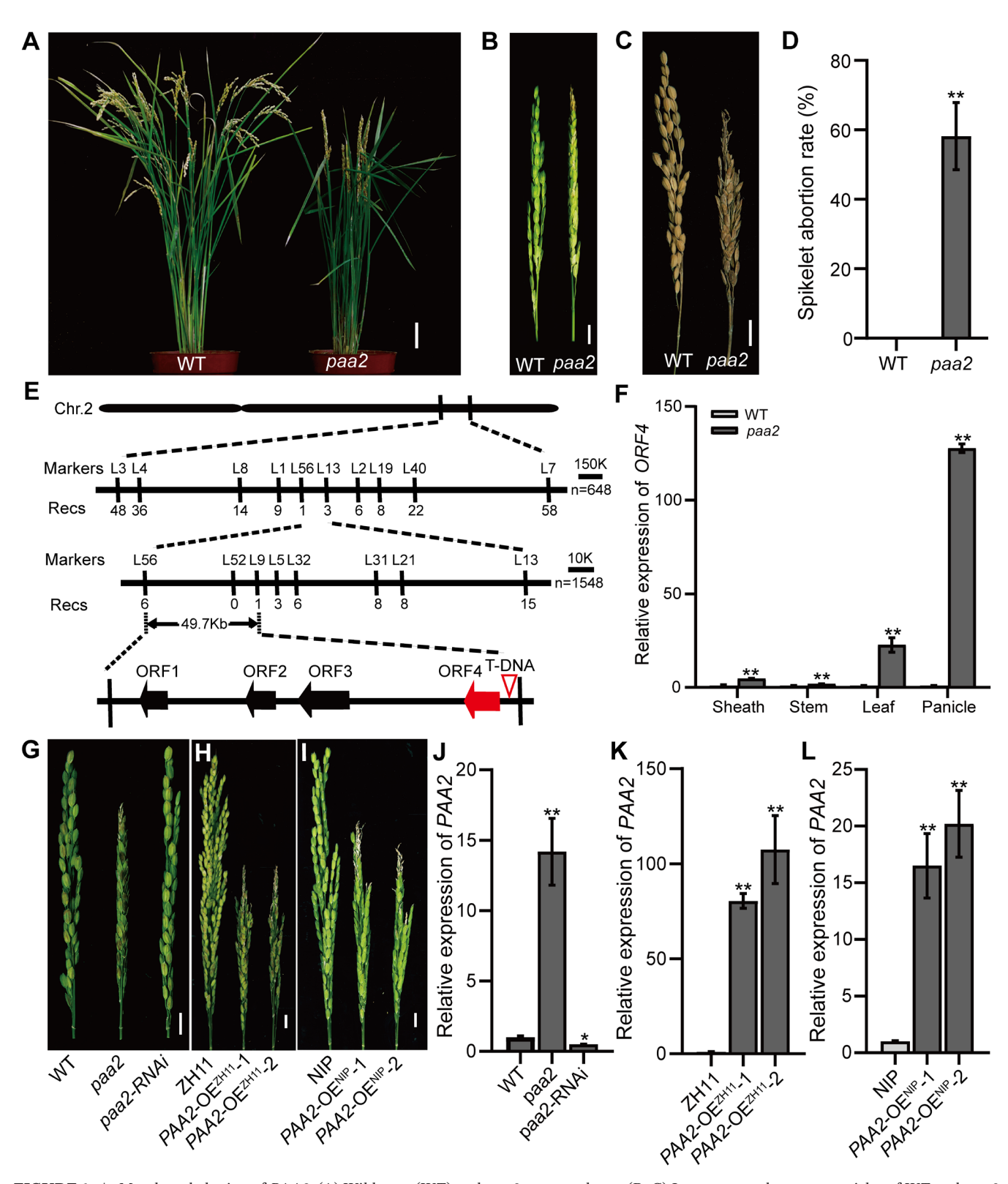


FIGURE 1 | Map-based cloning of PAA2. (A) Wild type (WT) and paa2 mutant plants. (B, C) Immature and mature panicles of WT and paa2 mutant. (D) Spikelet abortion rates in WT and paa2 mutant ($n \ge 15$). (E) Fine mapping of PAA2. The molecular markers and corresponding numbers of recombinants are indicated above and below the black line, respectively. The candidate ORF is highlighted with a red arrow. The red triangle represents the position of inserted T-DNA. (F) Relative expression of ORF4 in different tissues of WT and paa2 mutant (n = 3). (G-L) Confirmation of PAA2 gene candidate by RNA interference to ORF4 (paa2-RNAi, G, J) and overexpression of ORF4 in Zhonghual1 (PAA2-OE^{ZH1}, H, K) and NIP (PAA2-OE^{NIP}, I, L). (G-I) Panicles of transgenic plants. (J-L) Relative expression of PAA2 in different transgenic plants (n = 3). Bars, 5 cm in (A), 1 cm in B, C and G-I. All data shown are means \pm SD. *p < 0.05, *p < 0

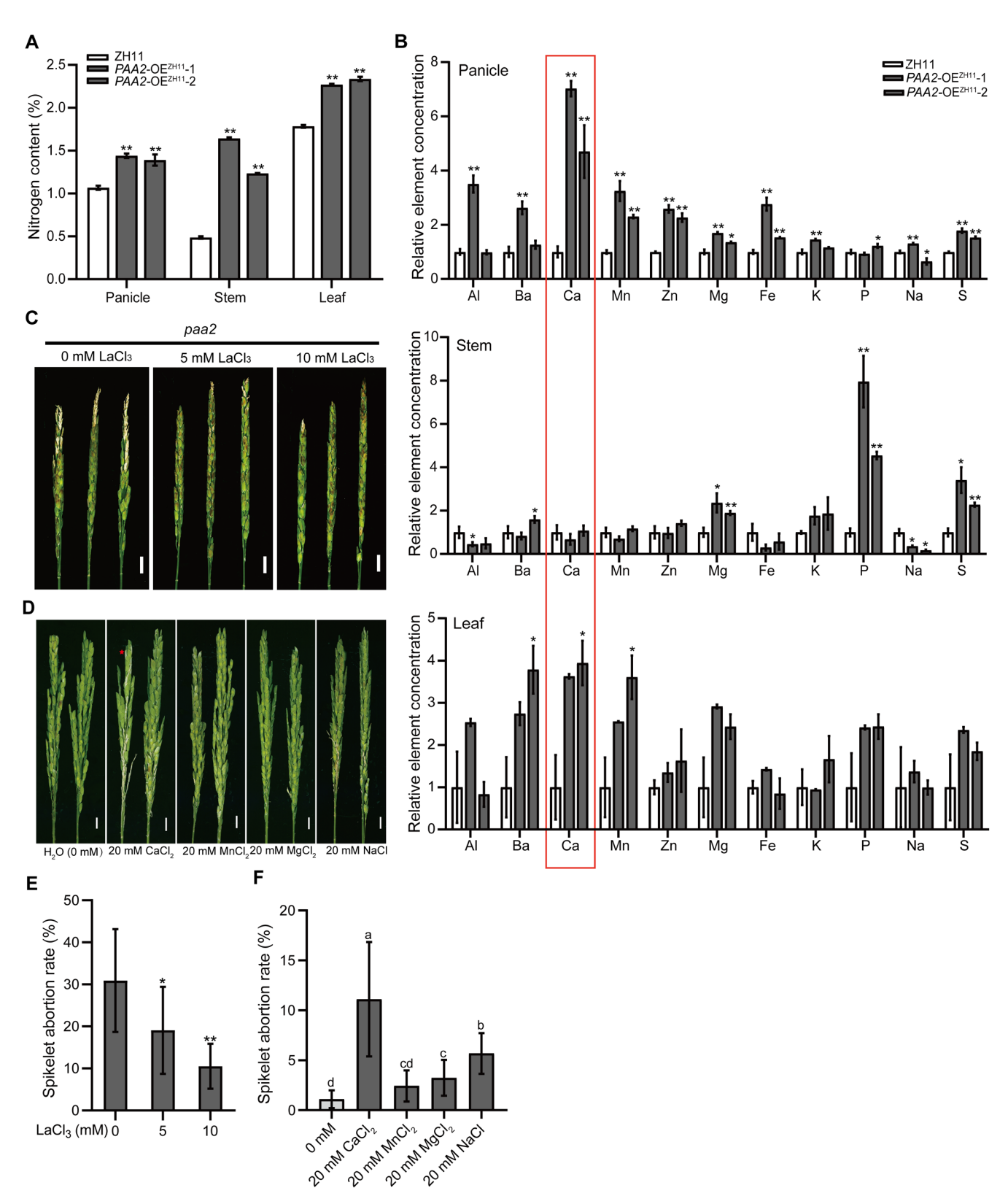


FIGURE 2 | High nitrogen accumulation and excessive calcium in plants overexpressing PAA2. (A, B) Nitrogen content and relative concentrations of various cations in panicles, stems and leaves of ZH11 and PAA2-OE^{ZH11} (n = 3). (C, E) Phenotypes (C) and corresponding spikelet abortion rates (E) for paa2 mutant panicles injected with water (control), and 5 and 10 mM LaCl₃, respectively. (D, F) Representative phenotypes (D) and spikelet abortion rates (F) for GSHD panicles injected with water (control), 20 mM CaCl₂, 20 mM MnCl₂, 20 mM MgCl₂ and 20 mM NaCl. Red star symbol represents apical spikelet abortion. Bars, 1 cm in C and D. All data shown are means \pm SD. Student's t-tests. $n \ge 8$, *p < 0.05, **p < 0.01. Different letters represent significant differences (p < 0.05 in Tukey's multiple comparisons tests).

Given that excessive intracellular Ca²⁺ is cytotoxic, we postulated that dramatically increased calcium in the panicles was the major cause of apical panicle abortion. For validation, we injected the calcium channel blocker LaCl, into young paa2 mutant panicles (about 3 cm in length) and evaluated the spikelet abortion. The numbers of aborted spikelets relative to total spikelets per panicle decreased from 30.92% (water treatment, CK) to 18.09% with 5 mM LaCl₃, and further to 10.53% with 10 mM LaCl₂ (Figures 2C,E and S4). Treatment with LaCl₂ in combination with EGTA (a calcium chelator) to young panicles of PAA2-OEZH11 plants rescued the abortion rate to a mild level (Figure S5). To further clarify which cation caused PAA, we injected several kinds of cation (Ca²⁺, Mn²⁺, Mg²⁺, K⁺, Na⁺) into both young panicles of GSHD and ZH11. The results showed each CaCl₂ treatment (10 or 20 mM) could lead to more panicle degeneration significantly than other cation treatments; specifically, distinct PAA phenotype appeared after 20 mM CaCl₂ exogenous application (Figures 2D,F and S6). Together, these results suggested that excessive cations, especially Ca²⁺, were responsible for apical panicle abortion in the paa2 mutant.

2.3 | PAA2 Transports Cations in Oocytes

As OsNPF7.9 is a low-affinity nitrate transporter (Guan et al. 2022), we investigated whether PAA2 also responds to and transports cations. We initially found that exogenous CaCl, significantly upregulated PAA2 expression (Figure S7), hinting at a cation-related function. We then used two-electrode voltage clamp (TEVC) in Xenopus laevis oocytes to assess cation permeability. PAA2-cRNA-injected oocytes exhibited substantially larger inward currents than water-injected controls (Figure 3A,B). These currents displayed a dose-dependent increase with rising external CaCl, concentrations, indicating Ca²⁺ permeability (Figure 3C,D). X. laevis oocytes endogenously express Ca2+-activated chloride channels (CaCCs) (Schroeder et al. 2008). Therefore, Ca²⁺ influx mediated by PAA2 could potentially activate CaCCs, leading to Cl⁻ efflux that contributes to the observed inward current. Application of the CaCC inhibitor 4,4'-diisothiocyanatostilbene-2,2'-disulfonic acid (DIDS) at saturating concentrations to dissect the PAA2-mediated current revealed a DIDS-insensitive inward current that was subsequently abolished by the Ca²⁺ channel blocker LaCl₃ (Figure 3E,F), thus confirming direct Ca²⁺ conduction by PAA2.

To further investigate whether PAA2 has cation selectivity, we tested other divalent and monovalent cations (Ba $^{2+}$, Mg $^{2+}$, K $^{+}$ or Na $^{+}$) that do not activate CaCCs. PAA2-expressing oocytes displayed distinct inward currents in the presence of each of these cations, although with varying amplitudes (Figure 3G,H). These results demonstrate that PAA2 also conducts Na $^{+}$, Ba $^{2+}$, K $^{+}$ and Mg $^{2+}$ and establishes that PAA2 functions as a transporter for Ca $^{2+}$ and a range of other cations, expanding its physiological role beyond nitrate transport.

2.4 | Overexpression of *PAA2* Impairs Indigenous Calcium Ion Homeostasis Within Panicles

To investigate calcium ion homeostasis in panicles, calcium ion concentrations were measured longitudinally by dividing

a developing panicle into terminal, middle and base portions in *Japonica* cv. GSHD. The highest concentration of calcium was initially in the base portion of the young panicle (< 5 cm length), gradually decreased until the heading stage. Conversely, Ca²⁺ concentration in the terminal portion gradually increased, exceeding the concentration in the middle and base portions when the panicle length reached 7 cm and beyond. The upper portion retained a high level of calcium until heading. Calcium concentration in the middle portion gradually increased until heading, exceeding the concentration in the base portion when the panicle was about 15 cm in length. Thus, a distinct short-term terminal-focused Ca²⁺ gradient emerged in panicles from 13 cm until heading and disappeared after heading (Figure 4A).

We investigated the Ca2+ concentration gradient at the preheading, heading and grain fill stages in PAA2-OEZH11 plants. At pre-heading (about 13 cm), both wild type and PAA2-OE^{ZH11} panicles displayed tip-focused calcium ion gradients, whereas the wild type showed no difference between adjacent portions. However, a higher concentration of Ca²⁺ appeared in the upper portion of the PAA2-OEZH11 panicle, indicating that excessive calcium ion accumulation was already occurring at this stage. The Ca²⁺ gradient disappeared in the panicle of the wild type at heading, whereas panicles of PAA2-OEZH11 retained Ca²⁺ gradients until the grain-fill stage (Figure 4B). As a reliable non-destructive technique for metal elemental analysis, microfocus X-ray fluorescence (µ-XRF) scanning has been employed in valuating calcium distribution within rice seeds (Liu et al. 2024). We further investigated calcium ions distribution on both young panicles of ZH11 and PAA2-OE^{ZH11} using the μ-XRF scanning technique. Compared with ZH11, we found stronger fluorescence intensity appeared at the top of the PAA2-OEZH11 panicle from PL7 and PL9 rather than PL5 (Figure 4C,D), suggesting a higher Ca²⁺ accumulation at the top of the panicle from PL7 on, thus forming a tipfocused calcium concentration gradient.

Transmission electron microscopy (TEM) and terminal deoxynucleotidyl transferase-mediated dUTP nick-end labeling (TUNEL) analysis of the time point at which apical panicle abortion started to occur indicated that most of the PAA accumulated at the panicle differentiation stage (< 5 cm) (Figure 4E,F), synchronised with the PAA phenotype at the stage about PL5 (Figure S8A), accompanied by the accumulation of hydrogen peroxide and programmed cell death (PCD) in terminal panicle cells (Figure S8B-F).

2.5 | Spatiotemporal Expression Pattern of *PAA2* Matches to Its Potential Function in Tip-Focused Cation Transportation

OsNPF7.9 is expressed mainly in xylem parenchyma cells within vasculature, and OsNPF7.9 is plasma membrane-localised (Guan et al. 2022). To explore whether the spatiotemporal expression pattern of PAA2 aligns with its function in acropetal calcium ion transportation, we investigated the PAA2 expression pattern in adult plants. As expected, PAA2 was slightly expressed in young panicles at 5 cm in length and highly expressed in panicles with developed vasculature (15–19 cm in length) (Figures 5A and

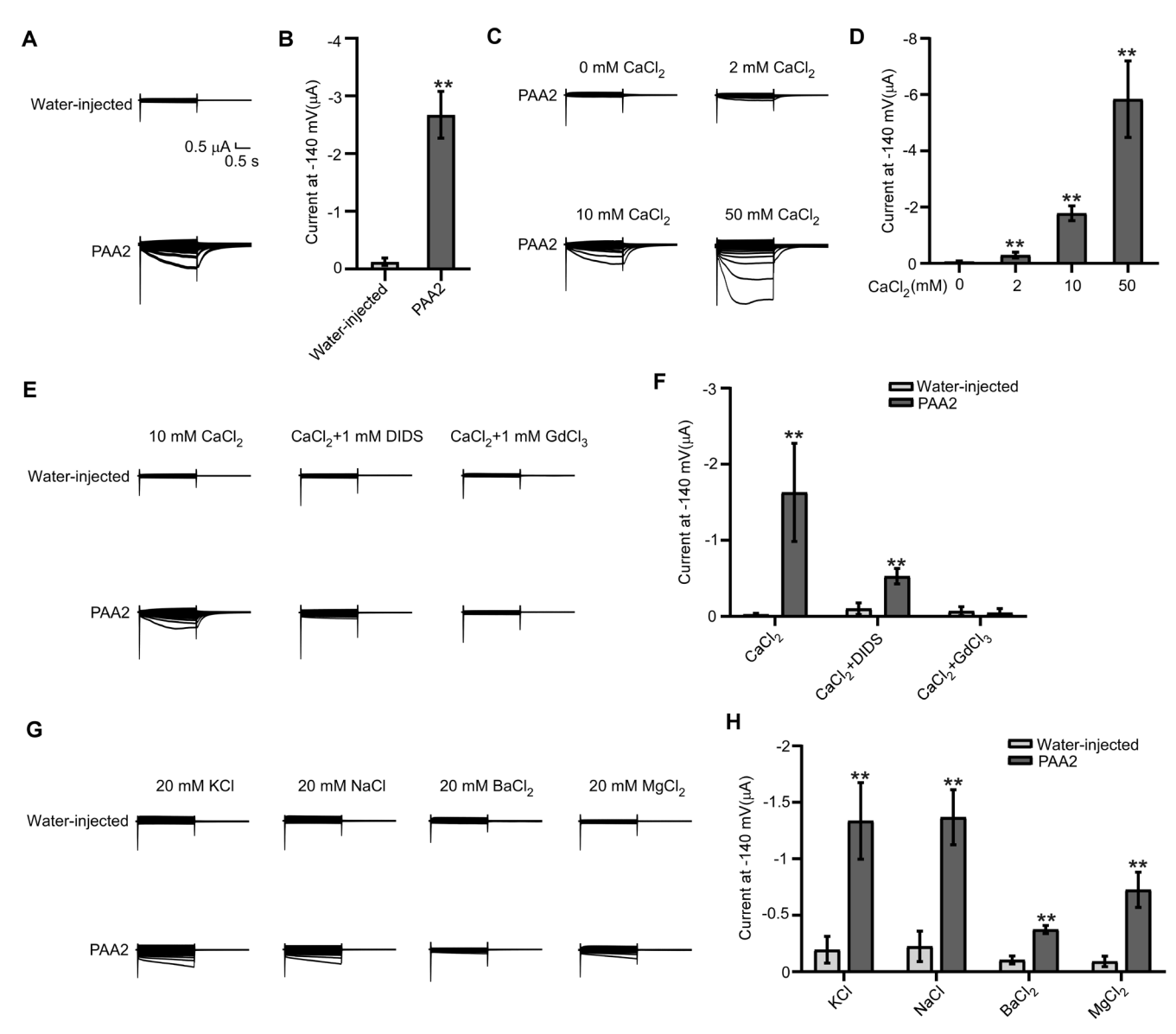


FIGURE 3 | PAA2 mediates Ca^{2+} transport in *Xenopus* oocytes. (A) TEVC recording from oocytes injected with water (control) or oocytes expressing PAA2 in the bath solution containing 20 mM $CaCl_2$. (B) Current amplitudes at -140 mV from multiple recordings as in (A). (C) TEVC recording from *Xenopus* oocytes expressing PAA2 in bath solutions containing water, 2, 10 or 50 mM $CaCl_2$. (D) Current amplitudes at -140 mV from multiple recordings in (C). (E) Oocytes expressing PAA2 or oocytes injected with water were recorded in the solution containing 10 mM $CaCl_2$ plus 0.1 mM 0.1 mM

S9). mRNA in situ hybridisation to explore whether *PAA2* is expressed at the initial stage of panicle differentiation showed that *PAA2* transcripts started to appear in the shoot apical meristem. Transcripts then became abundant and moved to the branch meristem, followed by the spikelet meristem, and finally disappeared after completion of panicle differentiation (about 1 cm in length, Figure 5B), indicating that besides expressing in vascular bundle tissue, *PAA2* can also express briefly in the apical part of the young panicle. Mutant *paa2* has a higher expression level in the panicle (Figure 1F). To survey whether the higher expression level caused higher calcium accumulation, we detected its calcium ion concentration using a cell-permeable calcium ion indicator Fluo-4/AM (Qiu et al. 2020). As expected, a strong

fluorescence in the *paa2* mutant revealed that a higher *PAA2* expression level facilitates the upward transport of calcium ions from the stem to the young panicle, even without visibly developed vascular tissue (Figure 5C).

When expressed in transient assays in *N. benthamiana* and rice protoplasts, PAA2-GFP co-localised with the plasma membrane (PM) marker PIP2-mCherry, (ER) marker HDEL-mCherry, prevacuolar compartment (PVC) marker VSR2, and even with vesicle-associated membrane protein VAMP727 (Figures 5D and S10). We also found that PAA2 interacted with VAMP727 in yeast two-hybrid (Y2H) assays, in vivo fluorescence luciferase (LUC) complementary imaging and co-immunoprecipitation

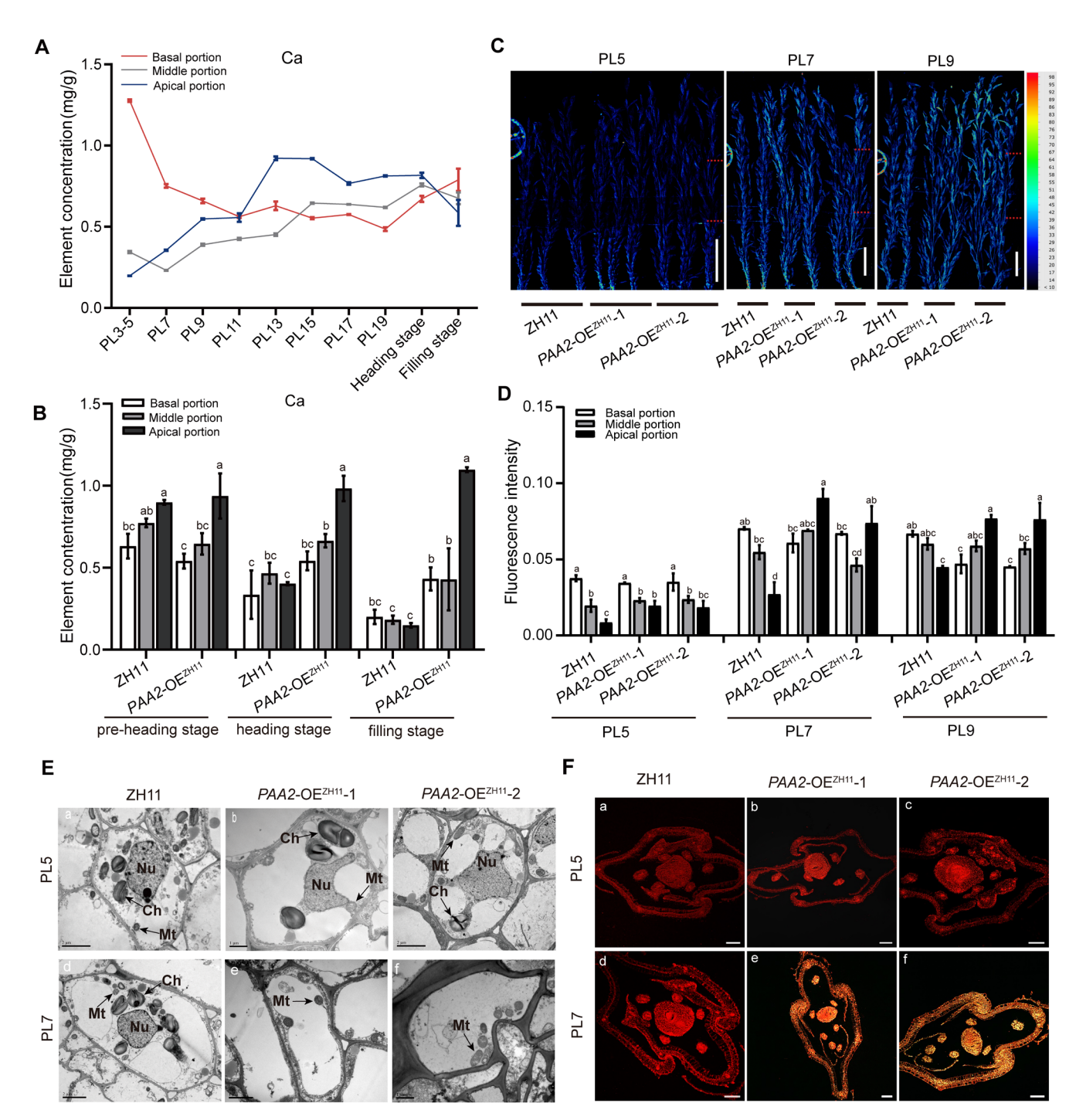


FIGURE 4 | Overexpression of *PAA2* disturbs calcium ion homeostasis in panicles and causes PAA. (A) Calcium ion concentrations in apical, middle and basal portions of panicles at different developmental stages (PL defined by panicle length in cm) in rice cv. GSHD. (B) Ca concentrations in panicles at pre-heading (13 cm), heading and grain fill stages of ZH11 and *PAA2*-OE^{ZH11} plants, respectively. (C) X-ray fluorescence (XRF) scan of panicles of ZH11 and *PAA2*-OE^{ZH11} at PL5, 7 and 9 development stages, respectively. The red and blue colours represent high and low Ca concentrations, respectively. The panicles were divided into apical, middle and base portions marked by red dashed lines. (D) Quantification of the fluorescence intensity of XRF images in (C). (E, F) Microscopic images and TUNEL assay in distal parts of panicles (5–7 cm) in ZH11 and *PAA2*-OE^{ZH11} plants. Nu, nucleus; Mt., mitochondrion; Ch, chloroplast. Bars, 10 mm in (C), 2 μm in (E) (a, c and d), 1 μm in (E) (b, e and f), 100 μm in (F). Data are means \pm SD (n = 3). Different letters represent significant differences (p < 0.05 in Tukey's multiple comparisons tests).

(Co-IP) experiments using *N. benthamiana* (Figure 5E–G). As a member of soluble N-ethylmaleimide-sensitive factor attachment protein receptors (SNAREs), VAMP727 is involved in trafficking cargo proteins to their final destinations, including the plasma membrane. In *Arabidopsis*, there is a VAMP727-mediated

secretory pathway for the delivery of secondary cell wall components to maintain the tubular morphology of root hairs (Hirano et al. 2023). Co-localisation and interaction of PAA2 with VAMP727 suggest that PAA2 transports calcium to extracellular spaces.

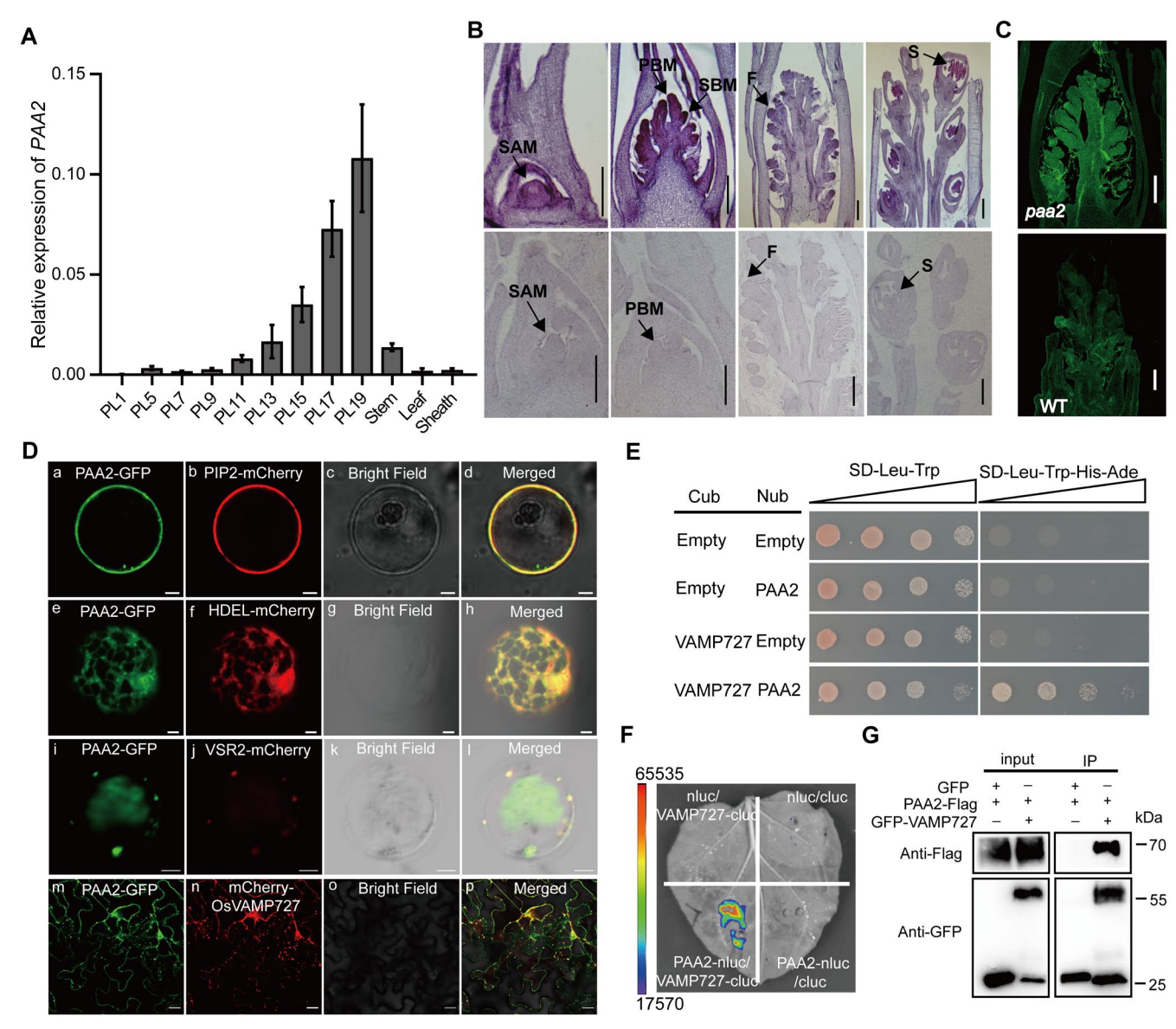


FIGURE 5 | Expression patterns of *PAA2*. (A) Expression of *PAA2* relative to *OsUbiquitin* in the stem, leaf and leaf sheath of an adult plant, and in panicles at different stages, defined by length of (1, 5, 7, 9, 11, 13, 15, 17 and 19 cm). Data are means \pm SD (n = 3). (B) RNA in situ hybridization of *PAA2* in young panicles. Arrows indicate *PAA2* expression sites. A *PAA2* sense probe was used as a negative control (bottom row). SAM, shoot apical meristem; PBM, primary branch meristem; SBM, secondary branch meristem; F, flower; S, stamen. (C) Fluorescent Fluo-4/AM stainness to the sections of *paa2* (upper) and its wild type (down), respectively. (D) Subcellular localization of PAA2. PAA2-GFP fusion protein was transiently co-expressed with the plasma membrane marker PIP2-mCherry, endoplasmic reticulum marker HDEL-mCherry and PVC marker VSR2-mCherry in rice protoplasts and SNAREs member VAMP727 in *N. benthamiana*. (E) PAA2 interacts with OsVAMP727 revealed by split-ubiquitin yeast two-hybrid assay. Yeast transformants were plated on SD medium either lacking Leu and Trp (SD/-Leu/-Trp) (left) or on SD medium lacking Leu, Trp, His and Ade (SD/-Leu/-Trp/-His/-Ade) (right), with the empty vector as a negative control. Triangles indicate concentration. (F) Firefly LCI assay of PAA2 combining VAMP727 in *N. benthamiana* leaf cells. cLUC, C terminus of LUC; nLUC, N terminus of LUC. Scale bar indicates the luminescence intensity in counts per second (CPS). (G) Co-IP assay of PAA2-FLAG and GFP-VAMP727 in *N. benthamiana* leaf cells. Bars, 250 μm in (B) and (C); 5 μm in (D) (a–l); 20 μm in (D) (m–p).

2.6 | PAA2 Interacts With OsUBC45 to Regulate Ca²⁺ Homeostasis

Excessive intracellular Ca²⁺ accumulation is cytotoxic. To explore the possibility that rice has a mechanism to regulate PAA activity, we performed Y2H screening and identified an interacting counterpart, OsUBC45 (Figure 6A). LUC complementary imaging (Figure 6B), Co-IP experiments (Figure 6C) and

BIFC assays (Figure S11) in *N. benthamiana* confirmed the authenticity of the interaction. Further investigation showed that *OsUBC45* was expressed throughout the entire period of panicle development (Figure S12A). In situ hybridisation at the initial stage of panicle differentiation indicated that OsUBC45 expression overlapped with PAA2 (Figure S12B). To understand their genetic relationship, we created *PAA2^{cri}* and *OsUBC45^{cri}* mutants, and the double *PAA2^{cri}/OsUBC45^{cri}* mutant in cv.

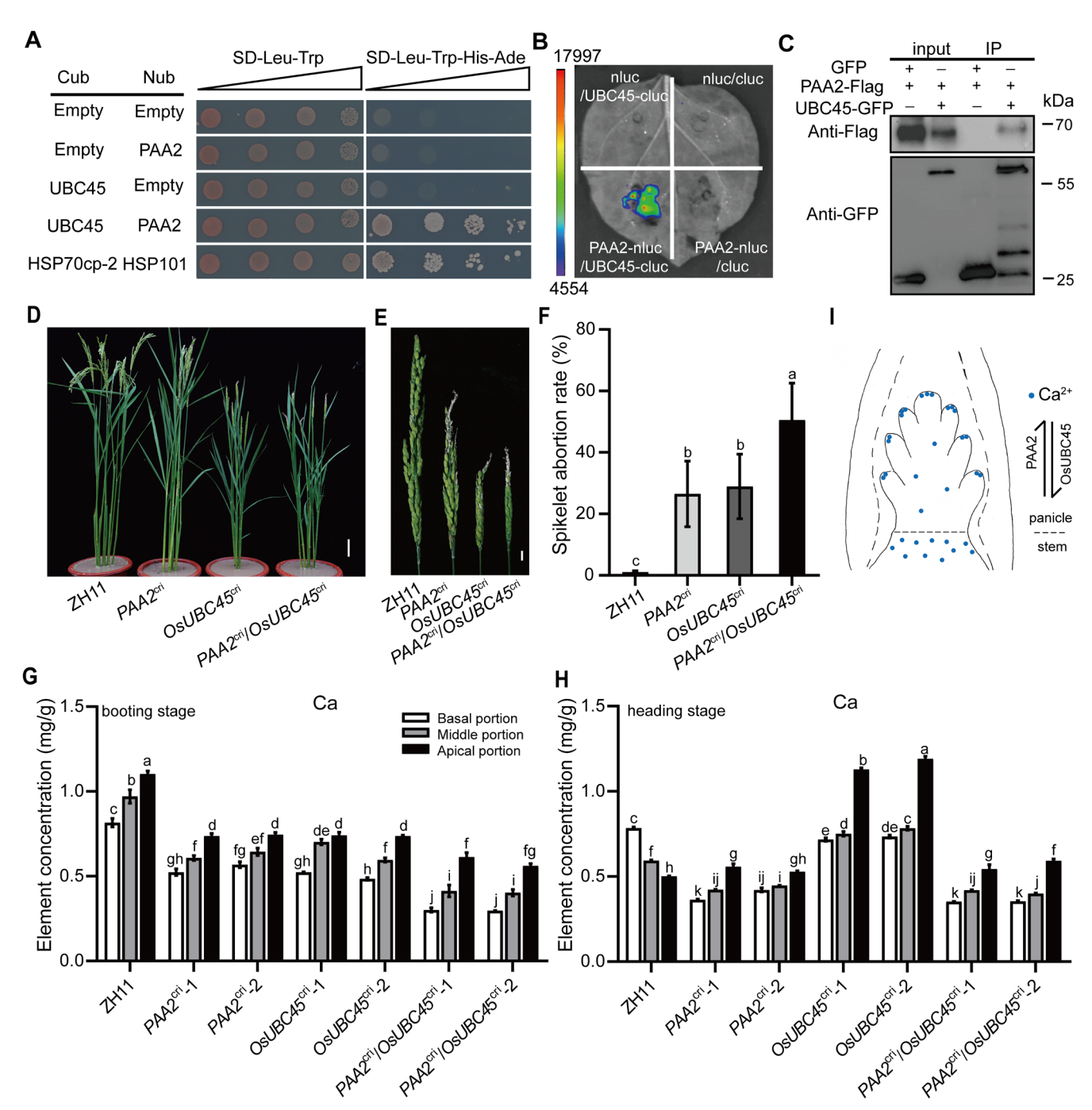


FIGURE 6 | PAA2 interacts with OsUBC45 to maintain Ca^{2+} homeostasis. (A) Split-ubiquitin yeast two-hybrid assay showing the interaction of PAA2 and OsUBC45. pXGY17-HSP70cp-2 and pXGY18-HSP101 were used as a positive control. (B) Firefly LCI assay showing the interaction in *N. benthamiana* leaf cells. (C) Co-IP assay showing that PAA2-FLAG co-precipitates with OsUBC45-GFP in *N. benthamiana* leaf cells. (D–H) Plant phenotypes (D), panicle phenotypes (E), spikelet abortion rates (F) and Ca^{2+} concentrations in different panicle parts at booting (G) and panicle emergence (H) in ZH11, $PAA2^{cri}$, $OsUBC45^{cri}$ and $PAA2^{cri}/OsUBC45^{cri}$ mutants, respectively. Bars, 5 cm in D, 1 cm in E. Data are means \pm SD. Different lowercase letters above bars indicate significant differences (p < 0.05 determined by Tukey's multiple comparison test). (I) A proposed PAA2-OsUBC45 module that stabilises Ca^{2+} homeostasis. At differentiation of the panicle, PAA2 expresses around various meristems of the panicle, facilitating the transportation of calcium ions from the basal portion towards the apex. After 13 cm in length, the panicle forms a short-term Ca^{2+} gradient. This process is constrained by UBC45. Overexpression of PAA2 or knockout of PAA2 disrupts PAA2 homeostasis, leading to excessive calcium accumulation, resulting in apical panicle abortion occurrence. Blue dots represent calcium ions.

Zhonghua11 using CRISPR/Cas9 technology (Figure S13A). Plant height, panicle length and grain number per panicle were slightly reduced in the *PAA2^{cri}* mutant, and greatly reduced in the *OsUBC45^{cri}* and *PAA2^{cri}/OsUBC45^{cri}* mutants compared

with the WT (Figure S13B–H). Although all three mutants showed PAA phenotypes, the symptoms for the *OsUBC45^{cri}* and *PAA2^{cri}/OsUBC45^{cri}* mutants were more severe, suggesting that UBC45 plays a more important role (Figure 6D–F). Assays

of calcium ion concentration in panicles at the pre-heading stage indicated significant reductions in all three mutants (Figure 6G). At 1 week post heading, the tip-focused calcium ion gradient was absent in the WT and weakened in the $PAA2^{cri}$ and $PAA2^{cri}/OsUBC45^{cri}$ mutants, whereas there was excessive calcium ion accumulation in the upper position of $OsUBC45^{cri}$ mutant panicles, similar to that in PAA2-OEZH11 lines (Figure 6H). These results suggest that OsUBC45 functions in a balancing role with PAA2 in maintaining Ca^{2+} homeostasis during panicle development.

3 | Discussion

Although PAA is an undesirable trait causing grain yield loss, it is still an interesting trait for studying panicle development (Cheng et al. 2011; Heng et al. 2018). Several studies showed that PAA affects multiple biological processes, including Ca²⁺ signal and transportation (Bai et al. 2015; Heng et al. 2018; Wang et al. 2018; Zafar et al. 2019; Ali et al. 2022; Peng et al. 2018; Gan et al. 2023). However, these documentations are fragmentary and insufficient to construct a systematic genetic network, and the molecular mechanisms underlying PAA remain elusive. In the present study, we characterised NO_3^-/Ca^{2+} symporter, PAA2, a member of the NPF transporter family that is homologous to Arabidopsis NRT1.5/AtNPF7.3 (Guan et al. 2022). The PAA2 protein is localised in the PM, ER and PVC, co-localises with VAMP727 and has the capacity for intercellular transportation of Ca²⁺. Our investigation revealed that Ca²⁺ homeostasis during panicle development was maintained by the PAA2-OsUBC45 module. Overexpression of PAA2 caused excessive accumulation of Ca²⁺ and disrupted homeostasis leading to apical panicle abortion. Interestingly, ym48 mutants decreased Ca²⁺ transport to the apical panicle, and Ca²⁺ deficiency also appeared as a degeneration phenotype (Gan et al. 2023). All these results suggest that calcium homeostasis within the rice panicle is essential for its normal development and provides a potential genetic modulating pathway for improving panicle type.

3.1 | PAA2 Is a Key Participant for Cation–Anion Balance

Irrespective of the form of nutrition, a very close balance was found in tomato between total cations (Ca²⁺, Mg²⁺, K⁺ and Na⁺) and total anions (NO₃⁻, H₂PO₄⁻, SO₄²⁻, Cl⁻), namely, a cationanion balance (Kirkby and Mengel 1966) that is attributed to the need for plants to maintain electroneutrality, although the underlying mechanism is still unclear. In this study, PAA2 was identified as a symporter of NO₃⁻ and other cations such as Ca²⁺, Na+, Ba2+, K+ and Mg2+. These cations were excessively accumulated in panicles either overexpressing PAA2 or carrying an OsUBC45 knock-out mutation, indicating that PAA2 is a participant in cation-anion balance. Although our results established that PAA in paa2 mutant and PAA2-OEZH11 lines was caused mainly by excessive Ca2+ accumulation, we also identified symptoms of excessive Mn2+ characterised by dark brown necrotic spots (Shrestha et al. 2018). Investigation of the dynamics of cation concentration showed that Mn²⁺ and Ca²⁺ shared similar tip-focused concentration gradients (Figure S14), suggesting the existence of Mn^{2+} homeostasis. We still lack knowledge of how PAA2 selects ions and allocates transportation capacity or whether the transportation is simply driven by transpiration.

3.2 | PAA2 Participates in Establishing a Tip-Focused Ca²⁺ Gradient in Young Panicles

Ca²⁺ gradients appear to be essential for polarised growth of both pollen tubes and root hairs (Hepler et al. 2001). In the present study, we show that calcium accumulation in rice panicle starts from the stage of differentiation of meristematic panicle tissue until the completion of meiosis (about 13 cm in length). Thereafter, a short-term tip-focused Ca²⁺ gradient emerges and remains until panicle emergence. From a morphological point of view, the acropetal pattern in young rice panicles is similar to that in pollen tube and root hairs growth. The panicle development is led by cell division and expansion in apical inflorescence meristems. After reaching 4cm, young rice panicles have completed differentiation of primary branches, secondary branches and spikelets. The rachis and branches then elongate exponentially until heading and flowering (Ikeda et al. 2004). At 5-13cm, rice panicles are at the most rapid elongation period with an average daily elongation of 2-3 cm. We infer from the present results that at the initial stage, PAA2 drives the tipfocused calcium ion accumulation until the completion of panicle differentiation. Considering that PAA2 also expresses in vascular bundles (Guan et al. 2022), increasing the expression level in >11 cm panicles may be attributed to the generation of new vascular bundles. However, the low expression level of PAA2 detected in panicles at 5-11 cm is inconsistent with dramatic tip-focused calcium accumulation, suggesting the participation of other unidentified calcium gradient-related factors. The viewpoint is supported by the calcium ion gradient in PAA2cri, at booting stage, a clear calcium ion gradient remains despite less calcium ions accumulation; however, a failure on calcium ion gradient disappearance at heading stage thus provides extra evidence of PAA2 as a crucial factor on Ca²⁺ homeostasis.

3.3 | A PAA2-OsUBC45 Module Participates in Maintaining Ca²⁺ Homeostasis

We identified OsUBC45 as an interacting protein with PAA2 in regulating calcium homeostasis in rice panicles. As a homologue of the ERAD-related E2 ubiquitin conjugating enzyme 32 in Arabidopsis possibly involved in the degradation of misfolded or incompletely folded proteins in the ER (Strasser 2018), OsUBC45 is involved in various biological processes. It regulates grain size and weight by interacting with RING-type E3 ubiquitin ligase DGS1 (decreased grain number 1) (Li et al. 2023) or combining glycogen synthase kinase 3 (OsGSK3) as well as plasma membrane-localised aquaporin OsPIP2;1 to promote their degradation (Wang, Yue, et al. 2023). Interaction between PAA2 and OsUBC45 suggests that OsUBC45 may target PAA2 for ubiquitination-mediated degradation. A similar in situ hybridisation signal as PAA2 in young panicle (<5cm in length) suggests their overlapped expression pattern. Moreover, as in PAA2^{cri} mutants, the Ca²⁺ gradient in the OsUBC45^{cri} mutant was disturbed. However, 1 week after heading, obviously excessive calcium accumulation in OsUBC45cri mutants paralleled

that in *PAA2*-OE^{ZH11} mutants, suggesting that OsUBC45 acts as a balancer of PAA2 and both are essential for maintaining Ca²⁺ homeostasis during panicle development (Figure 6I).

4 | Materials and Methods

4.1 | Plant Materials and Growing Conditions

The rice *paa2* mutant was identified from a HTF (hybrid transcription factors) library (Zhao et al. 2015). All parents, mapping populations and transgenic plants were grown in experimental fields at Beijing (116°130′ E, 39°54′ N) and Hainan (109°10′ E, 18°21′ N). *N. benthamiana* plants were grown in an artificial climate chamber (24°C, 16 h light/8 h darkness). Seedlings employed for gene expression assays were grown in hydropic nutrient solution (pH 5.5) modified from the solution of Yoshida et al. (1976). Prior to the RNA extraction, seedlings were pretreated with different concentrations of CaCl₂ for 24 h.

4.2 | TEM and TUNEL Analysis

For TEM, apical spikelets of the WT and *PAA2*-OE^{ZH11} lines at different developmental stages (panicle lengths, 5, 7 and 9 cm) were fixed in 2.5% glutaraldehyde fixation solution, pumped with a vacuum pump for 30 min, centrifuged at 12 000 rpm for 5 min and placed at room temperature for more than 24 h. All samples were rinsed three times with 0.1 M phosphate buffer (pH 7.0) for 10 min each time and fixed in a 1% osmic acid solution for 4 h. The fixed samples were dehydrated by ethanol gradient (30%, 50%, 70%, 90% and 100%) for 10 min each time. After dehydration, being coated and polymerised, the samples were sliced and stained with uranyl acetate and lead citrate prior to transmission electron microscopy (H7500 TEM; Japan).

For TUNEL analysis, apical spikelet hulls of WT and *PAA2*-OE^{ZH11} panicles at 5, 7 and 9 cm were fixed in FAA fixation solution, pumped by vacuum pump and placed at 4°C for more than 24h. The sample was embedded in paraffin, sliced and baked for 4 days. This was followed by dewaxing and rehydrating, washing, treatment with protease K and soaking in phosphate-buffered saline (PBS). The TUNEL assay was performed with a DeadEnd Fluorometric TUNEL kit (G3250; Promega) according to the manufacturer's instructions. Samples were observed with a confocal laser-scanning microscope (LSM980; ZEISS). Fluorescein and propidium iodide were detected using excitation/emission spectrum at 488/520 and 535/620 nm, respectively.

4.3 | DNA Laddering Analysis

Apical spikelets at different developmental stages (3, 5, 7, 9, 11 and 13cm panicle length) were ground into powder. Fragmented 100–200 bp DNA molecules were extracted using an Apoptotic DNA Ladder Extraction Kit (C0008; BIYUNTIAN Biotechnology). The fragmented DNA was separated by 2% agarose gel electrophoresis and captured under UV light.

4.4 | H₂O₂ Content and CAT Activity

The $\rm H_2O_2$ content and CAT activity in panicles were determined using an $\rm H_2O_2$ assay kit (S0038; Beyotime) and CAT assay kit (BC0200; Solarbio), respectively.

4.5 | Map-Based Cloning of PAA2

For map-based cloning of PAA2, an F_2 mapping population was generated from a cross of the paa2 mutant and japonica cv. IRAT129. New SSR and InDel molecular markers for fine mapping were developed by comparing the genomic sequences of the fine-mapped region between cv. Kitaake and IRAT129. To identify the candidate gene, annotation information provided by RGAP (http://rice.plantbiology.msu.edu/index.shtml) and Gramene (http://www.gramene.org) was used to predict genes within the fine-mapped interval. Primers listed in Table S1 were designed using primer design software Primer 3.0 (http://prime r3.ut.ee/).

4.6 | Subcellular Localisation of PAA2

The full-length CDS of *PAA2* was cloned into pAN580 to generate the pAN580-PAA2-GFP vector for subcellular localisation analysis. The CDS was inserted into pCAMBIA1305–GFP and further introduced into the *Agrobacterium tumefaciens* strain EHA105. The constructs were then transiently co-expressed in rice protoplasts or *N. benthamiana* leaves with the marker constructs in accordance with the methods described previously (Zhang et al. 2011; Li 2011). Images were captured using a confocal laser scanning microscope (LSM980; ZEISS). Primers are listed in Table S1.

4.7 | In Situ RNA Hybridisation of Rice Young Panicles

Young panicles were fixed in RNase-free FAA, dehydrated through a series of xylene and ethanol, embedded in paraffin and then longitudinally sectioned at $10\,\mu m$ thickness using a microtome (RM2245, Leica). A gene-specific fragment of the target gene coding region was cloned into the pGEM-T Easy vector (Promega) using primer pair ISH-PAA2 and ISH-OsUBC45, respectively. The amplified fragments were utilised to synthesise sense and antisense RNA probes. Probe labelling was performed using the DIG Northern Starter kit (cat. no. 2039672; Roche). In situ hybridisation was performed following Zong et al. (2022).

4.8 | RNA Isolation and RT-qPCR Analysis

Total rice RNA was extracted from tissues using a Quick-RNA Plant Miniprep Kit (cat. no. R2024; Zymo Research), in accordance with the manufacturer's instructions. First-strand cDNA was synthesised using a FastKing RT Kit (KR116; Tiangen). RT-qPCR was performed using TB Green Premix Ex Taq II FAST qPCR (cat. CN830A; TaKaRa) on an ABI PRISM 7900HT system (Applied Biosystems), using ubiquitin (Os03g0234200) as an

internal reference gene. Relative expression levels were calculated using the $2^{-\Delta\Delta Ct}$ method (Livak and Schmittgen 2001). The primers are listed in Table S1.

4.9 | Vector Constructs and Plant Transformation

A PAA2-RNAi construct was produced by cloning a 250 bp PAA2 fragment into pCUbi1390-ΔFAD2. To create the overexpression vector pUbi-PAA2, the full-length PAA2 CDS was inserted into binary vector pCUBi1390. To create CRISPR-Cas9 knockout vectors, 20 bp gene-specific spacers of target genes were separately cloned into the CRISPR-Cas9 to construct pCAS9-PAA2, pCAS9-OsUBC45 and pCAS9-PAA2/OsUBC45 vectors according to the method previously described (Miao et al. 2013). The resulting constructs were introduced into Agrobacterium tume-faciens strain EHA105 and transformed into the paa2 mutant (PAA2-RNAi), cv. Kitaake (pUbi-PAA2) and cv. ZH11 (pUbi-PAA2, pCAS9-PAA2, pCAS9-OsUBC45, pCAS9-PAA2/OsUBC45), respectively, according to a published procedure (Hiei and Komari 2008). The primers are listed in Table S1.

4.10 | Elemental Assay and Microfocus X-Ray Fluorescence (μ-XRF) Scanning

Rice leaves, stems and different lengths of young panicles were collected, dried at 65°C, ground into fine powder and digested into solution by a Hanon SH230N heavy metal digester. The heavy metal concentrations were determined using inductively coupled plasma optical emission (ICP-OES) (Agilent ICP-OES 5110).

To determine the panicle Ca concentration, panicles of ZH11 and PAA2-OE^{ZH11} at 5, 7 and 9 cm stage were collected and dried at 60°C for 3 days. Dried panicles were attached to double-sided carbon conductive tape and then scanned on an X-ray fluorescence (μ -XRF) spectrometer (M4 TORNADO PLUS, Bruker). The relative fluorescence intensities of μ -XRF images were quantified using ImageJ (https://imagej.net/ij/Download).

4.11 | Calcium Ion Fluorescence Staining

Young panicles of WT and paa2 were, respectively, fixed with 4% paraformal dehyde fix solution and then embedded in paraffin, sliced and baked for 4 days. The tissue sections were rinsed three times with PBS solution, then treated with 1 μ M Fluo-4/AM (S1060, Beyotime) solution containing 20% pluronic F-127 (ST501, Beyotime) and incubated in the dark at 37°C for 1h for loading fluorescent dye. After loading, the dye was washed three times with PBS solution to remove excess fluorescent dye and incubated at 37°C for 30 min, and observed with a confocal laser scanning microscope (STELLARIS 5, Leica).

4.12 | Calcium Channel Blocker Injections Into Developing Panicles

WT and paa2 mutant panicles at 1-3 cm were injected at the base with 1 mL of calcium channel blocker LaCl₃ (5 and 10 mM)

and repeated 4 days later. Different concentrations of cation solutions (containing Ca^{2+} , Mg^{2+} , Mn^{2+} , K^+ , Na^+) were, respectively, injected into the young panicles of GSHD and ZH11, and repeated after 4 days. Double distilled water was used as a control. The apical spikelet degradation rate was investigated after panicle emergence.

4.13 | Functional Characterisation of *PAA2* in *Xenopus laevis* Oocytes

The full-length *PAA2* CDS was cloned into *Eco*RI and *Bam*HI restriction sites in *Xenopus laevis* oocyte expression vector pGEMHE (Liman et al. 1992). After linearising the pGEMHE plasmid with *Bam*HI, the linearised DNA template was transcribed into capped cRNA using the T7 RiboMAX large-scale production system (Promega), and its purity and concentration were assessed for injection. Demembraned oocytes were isolated and injected with *PAA2* cRNA or diethyl pyrocarbonate-treated water using a microinjector and then incubated in ND96 bath solution at 16°C for 2–5 days. The ND96 solution was changed daily to maintain oocyte health. Electrical currents were recorded using the TEVC recording method. Oocytes were injected with diethyl pyrocarbonate-treated water as a negative control. Electrophysiological data were analysed with Clampfit software.

4.14 | Protein Interaction Assays

Y2H experiments were conducted according to Xu et al. (2017). The full-length CDS of *PAA2* was cloned into the Nub fragment in the pXGY18 vector, and the full-length CDS of *OsUBC45* was cloned into the Cub fragment in the pXGY17 vector.

For LUC complementation imaging (LCI) assays, the full-length CDS of *PAA2* and *OsUBC45* was cloned into pCAMBIA-Nluc or pCAMBIA-Cluc vectors, respectively. The resulting constructs were transformed into Agrobacterium strain EHA105 and transiently expressed in *N. benthamiana* leaves. LCI assays were performed as described (Chen et al. 2008).

For Bimolecular fluorescence complementation (BIFC) assays, the CDS of *PAA2* and *OsUBC45* were fused to p2YC or p2YN to generate PAA2-p2YC and OsUBC45-p2YN vectors, respectively. The plasmids were transformed into Agrobacterium strain EHA105 and transiently expressed in *N. benthamiana* leaves. BIFC assays were performed as described (He et al. 2023). YFP fluorescence signals were observed by confocal laser scanning microscope (LSM980; ZEISS).

Full-length CDS of PAA2 and OsUBC45 for Co-IP assays were cloned into pCAMBIA1300-FLAG or pCAMBIA1305-GFP vectors, respectively. All constructs were transiently expressed in N. benthamiana leaves, and subsequent experiments were conducted as previously reported (Zhang et al. 2024). Briefly, total protein from transformed leaves was extracted with lysis buffer (50 mM Tris-MES, pH8.0, 1 mM MgCl₂, 0.5 M sucrose, 10 mM EDTA, 5 mM DTT and $1 \times$ proteinase inhibitor cocktail, 0.4% Triton-X 100) and incubated with GFP-Trap magnetic beads (ChromoTek) at 4° C for 2 h. Western blots were conducted with

anti-GFP (11814460001, Roche, dilution 1:5000) and anti-FLAG (M185-7, MBL, dilution 1:5000) antibodies.

Author Contributions

Jianmin Wan and Zhijun Cheng supervised the project. Bojuan Liu and Zhijun Cheng designed experiments. Bojuan Liu, Sheng Luo, Wang Tian, Xin Liu and Jinhui Zhang performed most of the experimental work. Bujuan Liu, Zhijun Cheng and Xin Liu drafted the manuscript. Yulong Ren and Zebin Liu provided technical help with experiments. Jiale Shao and Yanqi Chang performed field work.

Acknowledgements

We are grateful for Xiaohong Zhu, Henan University, Kaifeng and Chuanyin Wu, Xianchun Xia, Institute of Crop Sciences, CAAS, for their critical review. We also acknowledge KeKe Yi, Institute of Agricultural Resources and Regional Planning, CAAS, for valuable suggestions.

Conflicts of Interest

The authors declare no conflicts of interest.

Data Availability Statement

The data that support the findings of this study are available on request from the corresponding author. The data are not publicly available due to privacy or ethical restrictions.

References

- Ali, A., T. K. Wu, H. Y. Zhang, et al. 2022. "A Putative SUBTILISIN-LIKE SERINE PROTEASE 1 (SUBSrP1) Regulates Anther Cuticle Biosynthesis and Panicle Development in Rice." *Journal of Advanced Research* 42: 273–287.
- Bai, J. T., X. D. Zhou, Q. Wang, et al. 2015. "Rice TUTOU1 Encodes a Suppressor of cAMP Receptor-Like Protein That Is Important for Actin Organization and Panicle Development." *Plant Physiology* 169: 1179–1191.
- Chen, H. M., Y. Zou, Y. L. Shang, et al. 2008. "Firefly Luciferase Complementation Imaging Assay for Protein–Protein Interactions in Plants." *Plant Physiology* 146: 368–376.
- Cheng, Z. J., B. G. Mao, S. W. Gao, et al. 2011. "Fine Mapping of *qPAA8*, a Gene Controlling Panicle Apical Development in Rice." *Journal of Integrative Plant Biology* 53: 710–718.
- Dong, Q. Y., L. Wallrad, B. O. Almutairi, and J. Kudla. 2022. " Ca^{2+} Signaling in Plant Responses to Abiotic Stresses." *Journal of Integrative Plant Biology* 64: 287–300.
- Drechsler, N., Y. Zheng, A. Bohner, et al. 2015. "Nitrate-Dependent Control of Shoot K Homeostasis by the Nitrate transporter1/Peptide Transporter Family Member NPF7.3/NRT1.5 and the Stelar K⁺ Outward Rectifier SKOR in Arabidopsis." *Plant Physiology* 169: 2832–2847.
- Gan, Q., F. S. Song, C. Z. Zhang, et al. 2023. " Ca^{2+} Deficiency Triggers Panicle Degeneration in Rice Mediated by Ca^{2+}/H^+ Exchanger OsCAX1a." *Plant, Cell & Environment* 46: 1610–1628.
- Gilliham, M., M. Dayod, B. J. Hocking, et al. 2011. "Calcium Delivery and Storage in Plant Leaves: Exploring the Link With Water Flow." *Journal of Experimental Botany* 62: 2233–2250.
- Guan, Y., D. F. Liu, J. Qiu, et al. 2022. "The Nitrate Transporter OsNPF7.9 Mediates Nitrate Allocation and the Divergent Nitrate Use Efficiency Between Indica and Japonica Rice." *Plant Physiology* 189: 215–229.
- He, Y. Q., S. Sun, J. Zhao, et al. 2023. "UDP-Glucosyltransferase OsUGT75A Promotes Submergence Tolerance During Rice Seed Germination." *Nature Communications* 14: 2296.

- Helper, P. K. 2005. "Calcium: A Central Regulator of Plant Growth and Development." *Plant Cell* 17: 2142–2155.
- Heng, Y. Q., C. Y. Wu, Y. Long, et al. 2018. "OsALMT7 Maintains Panicle Size and Grain Yield in Rice by Mediating Malate Transport." *Plant Cell* 30: 889–906.
- Hepler, P. K., L. Vidali, and A. Y. Cheung. 2001. "Polarized Cell Growth in Higher Plants." *Annual Review of Cell and Developmental Biology* 17: 159–187
- Hepler, P. K., and R. O. Wayne. 1985. "Calcium and Plant Development." *Annual Review of Plant Physiology* 36: 397–439.
- Hiei, Y., and T. Komari. 2008. "Agrobacterium-Mediated Transformation of Rice Using Immature Embryos or Calli Induced From Mature Seed." *Nature Protocols* 3: 824–834.
- Hirano, T., K. Ebine, T. Ueda, et al. 2023. "The SYP123-VAMP727 SNARE Complex Delivers Secondary Cell Wall Components for Root Hair Shank Hardening in Arabidopsis." *Plant Cell* 35: 4347–4365.
- Huang, Z., S. Ren, Y. Jiang, and T. Wang. 2016. "PINK1 and Parkin Cooperatively Protect Neurons Against Constitutively Active TRP Channel-Induced Retinal Degeneration in Drosophila." *Cell Death & Disease* 7: e2179.
- Ikeda, K., H. Sunohara, and Y. Nagato. 2004. "Developmental Course of Inflorescence and Spikelet in Rice." *Breeding Science* 54: 147–156.
- Jezek, M., and M. R. Blatt. 2017. "The Membrane Transport System of the Guard Cell and Its Integration for Stomatal Dynamics." *Plant Physiology* 174: 487–519.
- Kamiya, T., T. Akahori, M. Ashikari, and M. Maeshima. 2006. "Expression of the Vacuolar Ca^{2+}/H^+ Exchanger, OsCAX1a, in Rice: Cell and Age Specificity of Expression, and Enhancement by Ca^{2+} ." *Plant & Cell Physiology* 47: 96–106.
- Kirkby, E. A., and A. H. Knight. 1977. "Influence of the Level of Nitrate Nutrition on Ion Uptake and Assimilation, Organic Acid Accumulation, and Cation-Anion Balance in Whole Tomato Plants." *Plant Physiology* 60: 349–353.
- Kirkby, E. A., and K. Mengel. 1966. "Ionic Balance in Different Tissues of the Tomato Plant in Relation to Nitrate, Urea, or Ammonium Nutrition." *Plant Physiology* 42: 6–14.
- Li, H., M. Yu, X. Q. Du, et al. 2017. "NRT1.5/NPF7.3 Functions as a Proton-Coupled H⁺/K⁺ Antiporter for K⁺ Loading Into the Xylem in *Arabidopsis*." *Plant Cell* 29: 2016–2026.
- Li, J., B. L. Zhang, P. G. Duan, et al. 2023. "An Endoplasmic Reticulum-Associated Degradation-Related E2-E3 Enzyme Pair Controls Grain Size and Weight Through the Brassinosteroid Signaling Pathway in Rice." *Plant Cell* 35: 1076–1091.
- Li, J. Y., Y. L. Fu, S. M. Pike, et al. 2010. "The Arabidopsis Nitrate Transporter NRT1.8 Functions in Nitrate Removal From the Xylem Sap and Mediates Cadmium Tolerance." *Plant Cell* 22: 1633–1646.
- Li, X. Y. 2011. "Infiltration of *Nicotiana benthamiana* Protocol for Transient Expression via *Agrobacterium*." *Bio-Protocol* 1: e95.
- Liman, E. R., J. Tytgat, and P. Hess. 1992. "Subunit Stoichiometry of a Mammalian K⁺ Channel Determined by Construction of Multimeric cDNAs." *Neuron* 9: 861–871.
- Lin, S. H., H. F. Kuo, G. Canivenc, et al. 2008. "Mutation of the *Arabidopsis* NRT1.5 Nitrate Transporter Causes Defective Root-To-Shoot Nitrate Transport." *Plant Cell* 20: 2514–2528.
- Liu, H., C. Lu, X. Q. Liu, et al. 2024. "A Chloroplast Localized Heavy Metal-Associated Domain Containing Protein Regulates Grain Calcium Accumulation in Rice." *Nature Communications* 15: 9265.
- Livak, K. J., and T. D. Schmittgen. 2001. "Analysis of Relative Gene Expression Data Using Real-Time Quantitative PCR and the 2(-Delta Delta C(T)) Method." *Methods* 25: 402–408.

Miao, J., D. Guo, J. Zhang, et al. 2013. "Targeted Mutagenesis in Rice Using CRISPR-Cas System." *Cell Research* 23: 1233–1236.

Orrenius, S., B. Zhivotovsky, and P. Nicotera. 2003. "Regulation of Cell Death: the Calcium-Apoptosis Link." *Nature Reviews. Molecular Cell Biology* 4: 552–565.

Palanivelu, R., and D. Preuss. 2000. "Pollen Tube Targeting and Axon Guidance: Parallels in Tip Growth Mechanisms." *Trends in Cell Biology* 10: 517–524.

Peng, Y. B., F. X. Hou, Q. Bai, et al. 2018. "Rice Calcineurin B-Like Protein-Interacting Protein Kinase 31 (OsCIPK31) is Involved in the Development of Panicle Apical Spikelets." Frontiers in Plant Science 9: 1661.

Qiu, L. N., Y. Z. Wang, and H. Y. Qu. 2020. "Loading Calcium Fluorescent Probes Into Protoplasts to Detect Calcium in the Flesh Tissue Cells of *Malus domestica.*" *Horticulture Research* 7: 91.

Schroeder, B. C., T. Cheng, Y. N. Jan, and L. Y. Jan. 2008. "Expression Cloning of TMEM16A as a Calcium-Activated Chloride Channel Subunit." *Cell* 134: 1019–1029.

Shrestha, A., A. K. Dziwornu, Y. Ueda, L. B. Wu, B. Mathew, and M. Frei. 2018. "Genome-Wide Association Study to Identify Candidate Loci and Genes for Mn Toxicity Tolerance in Rice." *PLoS One* 13: e0192116.

Strasser, R. 2018. "Protein Quality Control in the Endoplasmic Reticulum of Plants." *Annual Review of Plant Biology* 69: 147–172.

Taochy, C., I. Gaillard, E. Ipotesi, et al. 2015. "The Arabidopsis Root Stele Transporter NPF2.3 Contributes to Nitrate Translocation to Shoots Under Salt Stress." *Plant Journal* 83: 466–479.

Thor, K. 2019. "Calcium-Nutrient and Messenger." Frontiers in Plant Science 10: 440.

Tian, W., C. Wang, Q. F. Gao, L. G. Li, and S. Luan. 2020. "Calcium Spikes, Waves and Oscillations in Plant Development and Biotic Interactions." *Nature Plants* 6: 750–759.

Wang, C., and S. Luan. 2024. "Calcium Homeostasis and Signaling in Plant Immunity." *Current Opinion in Plant Biology* 77: 102485.

Wang, C., R. J. Tang, S. H. Kou, et al. 2024. "Mechanisms of Calcium Homeostasis Orchestrate Plant Growth and Immunity." *Nature* 627: 382–388.

Wang, Q. L., A. Z. Sun, S. T. Chen, L. S. Chen, and F. Q. Guo. 2018. "SPL6 Represses Signalling Outputs of ER Stress in Control of Panicle Cell Death in Rice." *Nature Plants* 4: 280–288.

Wang, T., X. Y. Chen, C. F. Ju, and C. Wang. 2023. "Calcium Signaling in Plant Mineral Nutrition: From Uptake to Transport." *Plant Communications* 4: 100678.

Wang, Y., J. L. Yue, N. Yang, et al. 2023. "An ERAD-Related Ubiquitin-Conjugating Enzyme Boosts Broad-Spectrum Disease Resistance and Yield in Rice." *Nature Food* 4: 774–787.

Wang, Y. Y., and Y. F. Tsay. 2011. "Arabidopsis Nitrate Transporter NRT1.9 Is Important in Phloem Nitrate Transport." *Plant Cell* 23: 1945–1957.

White, P. J., and M. R. Broadley. 2003. "Calcium in Plants." *Annals of Botany* 92: 487–511.

Xu, Y., J. Yang, Y. H. Wang, et al. 2017. "OsCNGC13 Promotes Seed-Setting Rate by Facilitating Pollen Tube Growth in Stylar Tissues." *PLoS Genetics* 13: e1006906.

Yoshida, S., D. A. Forno, J. H. Cock, et al. 1976. *Laboratory Manual for Physiological Studies of Rice*. 3rd ed. International Rice Research Institute.

Zafar, S. A., S. B. Patil, M. Uzair, et al. 2019. "Degenerated Panicle and Partial Sterility 1 (DPS1) Encodes a Cystathionine β -Synthase Domain Containing Protein Required for Anther Cuticle and Panicle Development in Rice." New Phytologist 225: 356–375.

Zhang, B. L., Y. H. Wang, Y. Zhu, et al. 2024. "The MON1–CCZ1 Complex Plays Dual Roles in Autophagic Degradation and Vacuolar Protein Transport in Rice." *Journal of Integrative Plant Biology* 67: 35–54.

Zhang, Y., J. B. Su, S. Duan, et al. 2011. "A Highly Efficient Rice Green Tissue Protoplast System for Transient Gene Expression and Studying Light/Chloroplast-Related Processes." *Plant Methods* 7: 30.

Zhao, T., J. Liu, H. Y. Li, et al. 2015. "Using Hybrid Transcription Factors to Study Gene Function in Rice." *Science China. Life Sciences* 58: 1160–1162.

Zhou, J. G., Y. X. He, and X. Z. Meng. 2024. "Phosphorylation of CAX Transporters Controls Ca^{2+} Homeostasis." *Plant Communications* 5: 101042.

Zong, J., L. Wang, L. Zhu, et al. 2022. "A Rice Single Cell Transcriptomic Atlas Defines the Developmental Trajectories of Rice Floret and Inflorescence Meristems." *New Phytologist* 234: 494–512.

Supporting Information

Additional supporting information can be found online in the Supporting Information section. Figure S1: Statistical analysis of agronomic traits of the paa2 mutant. (A) Days to flowering (n = 10); (B) plant height $(n \ge 15)$; (C) tiller number $(n \ge 15)$; (D) panicle length $(n \ge 15)$; (E) grains per panicle $(n \ge 10)$; (F) grain length $(n \ge 10)$; (G) grain width $(n \ge 10)$; (H) 1000-grain weight (n = 3). Data are means \pm SD. **p < 0.01, Student's t-tests. Figure S2: Functional prediction and gene expression levels of open reading frames identified in the delimited region. (A) Genes within the region delimited by Indel markers of L56 and L9 and their putative functions. (B) Structure of LOC_Os02g46460. The white and black rectangles indicate untranslated regions and exons, respectively, and black lines represent introns. Black triangle indicates the T-DNA insertion position. PF, PR1 and PR2 are primers designed to identify the T-DNA insertion. (C) Agarose electrophoresis confirmation of T-DNA insertions. DNA fragments amplified using PF and PR1 or PF and PR2 primer pairs are indicated in (B). (D and E) Relative expression of ORF2 and ORF3 in different tissues of WT and paa2 mutant, respectively. Data are means \pm SD (n = 3). *p < 0.05; **p < 0.01, Student's t-tests. Figure S3: Plant phenotypes of overexpressing PAA2 in Zhonghua11 (A) and Nipponbare (B) backgrounds, respectively. Bars, 10cm in A and B. Figure S4: Plant phenotypes of paa2 after injection of calcium channel blockers. Red stars represent injected panicles. Two insets show the enlarged area on the uninjected (left) and injected (right) panicle indicated by white arrows. Bars, 5 cm. Figure S5: Injection of calcium channel blocker into PAA2-OEZH11 plants alleviates apical panicle abortion. (A) Plant phenotypes of PAA2-OEZH11 after injection of calcium channel blockers. Red star symbol represents injected panicles. White dotted arrow indicates the enlargement of area. (B) Representative PAA2-OEZH11 panicles after injection with water (control), and paired water and 5 and 10 mM LaCl₃+EGTA. (C) Spikelet abortion rates in PAA2-OEZH11 panicles following injection. Data are means \pm SD $(n \ge 10)$. *p < 0.05, Student's t-test. Bars, 10 cm in A, 1 cm in (B). **Figure** S6: Injection CaCl, into wild-type ZH11 and GSHD plants leads significant panicle abortion. (A) and (C) Representative GSHD (A) and ZH11 (C) panicles after injection with water (control), 10 mM CaCl₂, 10 mM MnCl₂, 10 mM MgCl₂, 10 mM KCl, 10 mM NaCl. Bars, 1 cm. (B) and (D) Degeneration rate in GSHD (B) and ZH11 (D) panicles with different solutions injection. Data are means \pm SD ($n \ge 8$). Different letters represent significant differences (p < 0.05 in Tukey's multiple comparisons tests). Figure S7: PAA2 expression induced after CaCl₂ application to leaves. Data are means \pm SD (n = 3). **Figure S8:** (A) Representative panicle of ZH11 (left) and PAA2-OEZH11 (right) at the development stages of PL3 (a), 5 (b), 7 (c), 9 (d), 11 (e), 13 (f) and 15 (g), respectively. Bars, 1 cm. (B–F) Programed cell death in distal regions of PAA2-OE $^{\rm ZH11}$ panicles was is confirmed by DNA laddering analysis (B), H_2O_2 contents (C), CAT activity (D) and expression levels of representative genes OsVPE2 (E) and OsVPE3 (F). The DNA for laddering was sampled from apical panicles at panicle lengths (PL) 3, 5, 7, 9, 11 and 13 cm. Data are means \pm SD (n=3), *p<0.05, **p<0.01, Student's t-tests. **Figure S9:** The expression

levels of PAA2 in different panicle portions at different developmental stages. Data are means \pm SD (n=3). **Figure S10:** Subcellular localisation of PAA2 in N. benthamiana. Co-localisation of PAA2 with plasma membrane marker PIP2-mCherry, endoplasmic reticulum marker HDELmCherry and PVC marker VSR2-mCherry were transiently expressed in leaves of N. benthamiana. Bars, 20 µm in (A-D), 5 µm in (E-L). Figure S11: Interaction of PAA2 with UBC45 in an N. benthamiana BiFC assay. The N-terminal (nYFP) or C-terminal YFP (cYFP) were infused with UBC45 and PAA2, respectively, and were co-expressed in N. benthamiana leaf cells. PAA2-YFPC/YFPN, UBC45-YFPN/YFPC was used as negative control. Bars, 50 µm. Figure S12: Expression patterns of OsUBC45 in adult plant tissues and developing panicles. (A) Relative expression levels of OsUBC45 in panicles of varying lengths and tissues of adult plants (n=3). (B) RNA in situ hybridisation of OsUBC45 in a differentiating panicle. Arrows indicate OsUBC45 expression sites with OsUBC45 sense probe as negative control. Bars, 250 µm. Data are shown as means ± SD. **Figure S13:** Statistical analysis of agronomic traits in ZH11 and PAA2cri, OsUBC45cri and PAA2cri/OsUBC45cri mutants. (A) Deletion sites in PAA2 and OsUBC45 in respective knockout lines. sgRNA target sequence and the PAM sequence are highlighted in blue and orange, respectively. Red dotted line indicates nucleotide deletions related to ZH11. (B) Plant height $(n \ge 10)$; (C) tiller number $(n \ge 10)$; (D) panicle length $(n \ge 10)$; (E) grain number per panicle $(n \ge 10)$; (F) grain length (n=30); (G) grain width (n=30); and (H) 1000-grain weight (n=5) in the WT and mutants. Data are means \pm SD. Different lowercase letters above the bars indicate significant differences (p < 0.05) determined by Tukey's multiple comparisons test. Figure S14: Mineral concentration profiles at various panicles lengths in cv. GSHD: Mn (A), Zn (B), Mg (C), K (D), Na (E) and Fe (F), respectively. Data are shown as means \pm SD (n=3). **Table S1:** Primers used in this study.